HIGH AREA-TO-MASS RATIO OBJECT POPULATION ASSESSMENT FROM DATA/TRACK ASSOCIATION

Timothy Payne[1], Moriba Jah [2], Jason Baldwin[3] and Tom Kelecy[4]

[1]U.S. Air Force Space Command, 250 S. Peterson Blvd., Peterson Air Force Base, CO 80914, USA
[2] Air Force Research Laboratory (RV), 3550 Aberdeen Ave., SE, Kirtland AFB, NM 87117, USA [3] Schafer Corp., 2309 Renard Place SE, Suite 300, Albuquerque, NM 87106, USA, Email: jbaldwing@schaferalb.com
[4] The Boeing Company, 5555 Tech Center Drive, Ste. 400, Colorado Springs, CO 80919, USA, Email: thomas.m.kelecy@boeing.com

ABSTRACT

To date, the actual population of High Area-to-Mass Ratio (HAMR) objects in Deep Space is still un-quantified. These are objects having area-to-mass ratios (AMR's) in the range of around 0.1 m^2/kg to 20 m^2/kg and higher. Typical methods for population assessment using optical sensors either count number of detections per unit time, or employ a disparate sequence of methods to compute HAMR object trajectories, where these methods assume linearized dynamics and fixed-gate correlations. This paper provides results from a set of actual angles (line of sight) data on HAMR objects, where the initial orbit determination and follow-on data/track association is performed probabilistically and autonomously. Moreover, the data are not only used to infer trajectories but also simultaneously exploited for their information content relating to each detected object's albedo-area-to-mass ratio. The results show that the inferred HAMR orbital elements and area-to-mass ratio values (CrA/m), parametrically, can be derived autonomously and without a priori knowledge of the orbit and CrA/m states. This will aid in the correlation of large numbers of uncorrelated tracks.

1 INTRODUCTION AND BACKGROUND

Schildknecht, et al. [1] discovered a population of deep space objects thought to have origins from sources in the neighborhood of the geosynchronous orbit (GEO) belt. The international space community is actively involved in tracking and characterizing these objects as they pose a hazard to active satellites operating in the vicinity of the GEO stationary ring. The exact number of these objects is unknown, as the dim, time-varying magnitudes and orbital perturbations resulting from the combination of lunar-solar perturbations and solar radiation pressure (SRP) make them a challenge to track consistently and reliably via optical sensors. Many are either higher or lower than the GEO orbital altitude, and thus transit into and out of view of most optical tracking sites due to the longitudinal drift relative to an Earth-fixed reference frame. Radars are limited in their ability of acquiring and tracking small objects at the near GEO ranges.

Nevertheless, repeated tracking of individual objects is crucial to making long-term observations with sensors that will provide better characterization of the material makeup of these objects, and to produce long-term orbital histories that might allow the objects to be associated with specific objects of origin. The photometric and spectral characterization of these objects will help, not only to determine their origin, but to better determine and track their orbits through improved non-conservative force and torque modeling [2,3,4].

With the advent of optical systems that can see to fainter magnitudes, more tracklets – a short sequence of observation – will be collected on a larger number of unknown objects. Many of these are likely to be HAMR objects, and so techniques that enable rapid, and nearly autonomous data association and processing are needed. This paper summarizes work done to demonstrate techniques that can be applied toward this end. The optical data used is described which was collected on a set of actual HAMR objects. Previously determined orbit and SRP values for the objects are described and serve as a "truth" state for comparison with the data association and estimation techniques applied. The results are compared along with the assessment of the data association and estimation performance.

2 GEODSS HAMR DATA

Data for 26 HAMR debris objects have been collected for analysis over the past several years from the U.S. Air Force Ground-based Electro-Optical Deep-Space Surveillance (GEODSS) network. A two-week segment of data, January 7-21, 2010, were extracted and used for this analysis. As most of the tracked objects drift due to either being super-synchronous or sub-synchronous orbits, the data are more consistent in terms of observations follow-up for some objects than others, depending on the orbit drift and visibility to the sensors. Figure 1 depicts some ground-based sensors (including GEODSS) along with the ensemble ground tracks for the objects propagated over a 1 week period.

Proc. '6th European Conference on Space Debris'
Darmstadt, Germany, 22–25 April 2013 (ESA SP-723, August 2013)

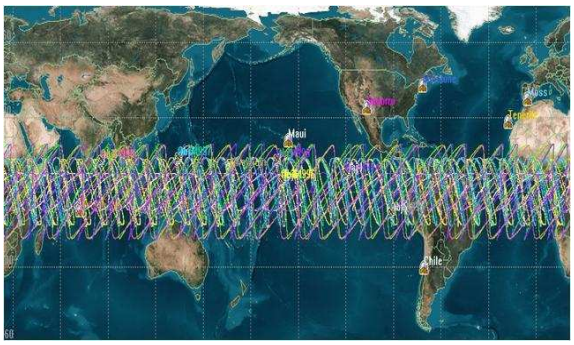

Figure 1. High Area-to-mass Ratio (HAMR) ground traces and selected ground sensor locations (including GEODSS).

The data are typically collected in "tracklets" when maintaining a known orbit. However, the amount – frequency and duration – can vary depending on whether or not a "new" object has been found and/or a better orbit estimate is desired. A histogram of the data intervals over the 2 week period is shown in Figure 2, where most of the data in a tracklet are separated by 5-20 seconds. Figure 3 shows the data history versus date where it can be seen that the average number of observations per day is around 150-250.

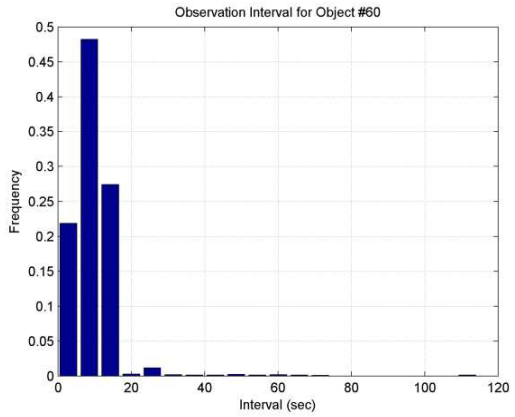

Figure 2. Data interval histogram for HAMR data collected over the 2 week period of January 7-21, 2010.

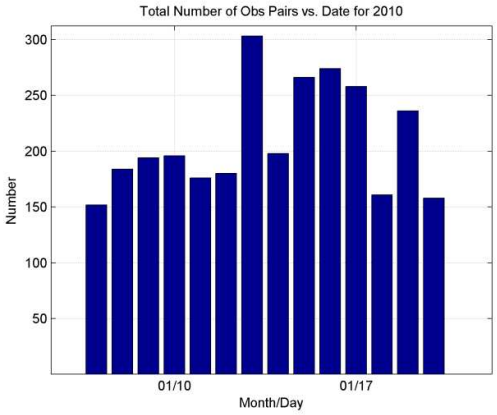

Figure 3. Data history for HAMR data collected over the 2 week period of January 7-21, 2010.

3 HAMR ATTRIBUTES

The data used to test the Constrained Admissible Region – Multiple Hypothesis Filter (CAR-MHF) process consists of up to 26 near GEO HAMR debris objects. Orbit and AMR solutions for each of these objects have been previously determined manually using the Orbit Determination Toolkit (ODTK) [5]. The results of that processing are used as "truth" references, and is summarized in Tables 1 and 2. Table 1 provides the average semi-major axis (Sma), inclination, eccentricity and AMR over the 2 year period 2009-2010, where the objects are categorized as "SubGEO" (sub-synchronous), "GEO" (near geosynchronous), and SupGEO (super-synchronous). The semi-major axes range from 33194 km to 46228 km, the inclinations from 6.4 degrees to 19.9 degrees, and the eccentricities from 0.011 to 0.275. The AMR values range from 0.0966 m^2/kg to 8.8805 m^2/kg. Table 2 shows the corresponding variations for each of the parameters over the period.

Table 1. Below is a list of 26 near GEO High Area-to-Mass Ratio (HAMR) objects whose orbits have been previously determined. The averages are over the 2009-2010 period.

HAMR Obj. #	Orbit Class	Sma (km)	Mean Motion (rev/day)	Avg. Inc. (deg)	Avg. Ecc	Avg. CrA/m (m^2/kg)
60	SubGEO	39990	1.0856	11.9	0.135	3.3397
61	GEO	42618	0.9868	14.7	0.011	0.0966
63	SubGEO	38230	1.1614	6.4	0.085	4.8805
64	SubGEO	40402	1.0691	8.8	0.071	4.3082
65	GEO	42239	1.0001	14.9	0.023	1.2224
67	GEO	41584	1.0238	13.2	0.045	0.9848
68	SubGEO	40790	1.0538	13.2	0.035	1.0441
71	GEO	41469	1.0281	13.2	0.016	0.8024
73	SubGEO	40374	1.0702	12.0	0.055	0.4887
77	GEO	41424	1.0297	13.0	0.045	2.0726
79	SupGEO	45135	0.9054	19.7	0.105	2.9519
80	GEO	41843	1.0143	7.8	0.038	2.8837
82	SubGEO	39729	1.0963	8.5	0.055	2.1366
83	SupGEO	44704	0.9185	16.8	0.090	2.0754
84	GEO	41922	1.0114	14.2	0.013	0.8814
85	GEO	42446	0.9928	14.7	0.040	0.4911
86	GEO	42448	0.9927	16.0	0.060	2.1654
87	SubGEO	33194	1.4355	10.0	0.275	3.6361
90	SubGEO	40121	1.0803	12.1	0.031	1.6873
93	SubGEO	40181	1.0779	10.9	0.095	1.5485
94	GEO	41311	1.0340	9.7	0.056	3.3049
95	GEO	41171	1.0392	13.9	0.035	2.7999
96	GEO	41308	1.0341	12.9	0.040	0.8366
97	GEO	41461	1.0284	13.4	0.014	0.7863
98	SupGEO	46228	0.8735	18.7	0.125	3.1332
99	SupGEO	44626	0.9209	19.9	0.095	1.3560

Table 2. Below is a list of 26 near GEO High Area-to-Mass Ratio (HAMR) objects and the variations in inclination, eccentricity and effective area-to-mass ratios over the 2009-2010 period.

HAMR Obj. #	Inc Var (deg)	Ecc Var (deg)	CrA/m Var (m^2/kg)	% CrA/m Change
60	0.9	0.110	0.01	0.3
61	0.2	0.003	0.07	72.5
63	1.7	0.150	0.06	1.2
64	0.7	0.139	0.22	5.1
65	0.1	0.034	0.75	61.4
67	0.2	0.030	0.18	18.3
68	0.1	0.030	0.70	67.0
71	0.3	0.029	0.33	41.1
73	0.2	0.010	0.27	55.2
77	0.6	0.071	0.35	16.9
79	0.1	0.050	0.03	1.0
80	1.0	0.064	0.01	0.3
82	0.8	0.070	0.07	3.3
83	0.1	0.060	0.11	5.3
84	0.1	0.015	0.01	1.1
85	0.1	0.020	0.18	36.7
86	0.1	0.080	0.09	4.2
87	0.1	0.010	0.05	1.4
90	0.2	0.059	0.09	5.3
93	0.8	0.050	0.45	29.1
94	1.2	0.108	0.03	0.9
95	0.1	0.010	1.20	42.9
96	0.2	0.020	0.70	83.7
97	0.3	0.013	0.26	33.1
98	0.1	0.050	2.30	73.4
99	0.5	0.050	0.02	1.5

Figure 4 shows the distribution of mean motions versus inclination, and Figure 5 the mean motion versus eccentricity. Figure 6 shows the ensemble variations in the AMR values in terms of the fractional (alternatively, percentage) variation relative to the mean AMR value for each object over the period 2009-2010. It should be noted that these variations represent the "effective area" relative to the sun, and some variations are a significant fraction of the average whereas some show minimal variability. It should also be noted that some of the variations have a periodic signature (at the scale of the sampling) whereas others are more random. This diversity of orbits and AMR values poses a challenge to space object tracking maintenance and prediction.

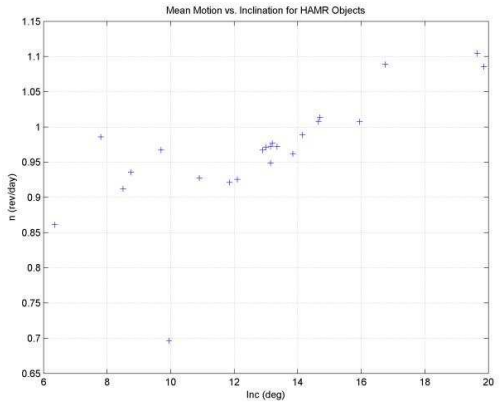

Figure 4. Mean motion versus inclination for the 26 near GEO HAMR objects.

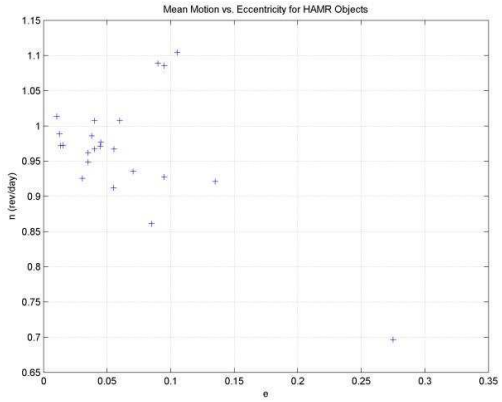

Figure 5. Mean motion versus eccentricity for the 26 near GEO HAMR objects.

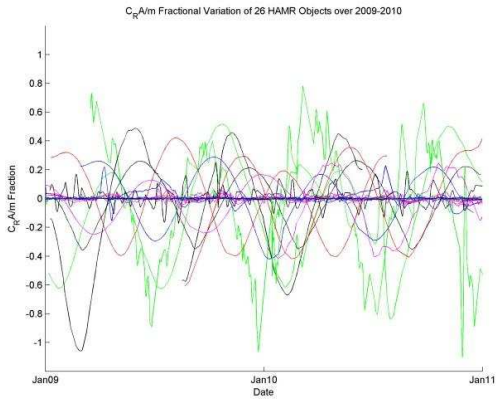

Figure 6. The ensemble fractional variations of effective area-to-mass ratio (relative to average) for the 26 near GEO HAMR objects over the 2009-2010 period.

4 CAR-MHF PROCESSING

The CAR-MHF processing flow is illustrated in Figure 7. The CAR process [6,7] initiates a set of filters when no existing estimates are available to process (i.e. when the available data are not associated to previously known objects, also called Un-Correlated Tracks [UCTs]). Existing estimates may be available from previous CAR generations. The CAR initiates a set of hypotheses based on data UCT and user supplied hypothesis constraints. Each hypothesis is propagated to the next measurement time. At that point, a probabilistic data association process is applied to one or more data pairs that might occur at a single time. If any measurements are associated to any hypotheses (based upon a Mahalanobis Distance criterion), all hypotheses for that object are updated with the associated measurement, and those updated are weighted based on their statistical likelihood as presented in [8,9]. In the case of an update, the hypothesis weights are adjusted accordingly and pruned based on user-selected criteria. If no update occurs, the hypotheses weights remain unchanged.

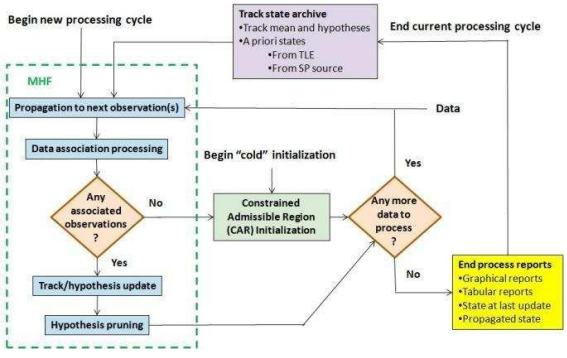

Figure 7. Depiction of the CAR-MHF process flow.

Conceptually, the data and hypothesis update approach enables multiple data to inform the filter which hypotheses are the most likely states. Each filter update further refines the hypotheses, rejecting the least likely, so ultimately the surviving hypothesis (or couple of hypotheses) is the converged state. The method can be thought of as an inductive process where states are hypothesized and the data are exploited for their ability to identify those hypothesized states that are statistically unlikely. It allows the user to only infer trajectories that are able to predict future observations. This process is depicted in Figure 8, where it should be noted that the Mahalanobis distance metric is the basis for the data association. Each hypothesis state and covariance at the measurement time is mapped to measurement space ("C" and "P" in Figure 8) and compared to the actual measurement at that time ("O" in Figure 8). The k^2 parameter is a chi-squared statistic that is compared against a user-specified probability limit for the purpose of data association determination (and is only statistically valid for distributions that are sufficiently Gaussian).

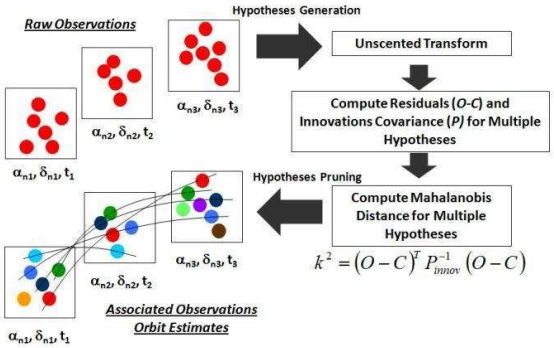

Figure 8. Conceptual depiction for multiple hypothesis and multiple data association processing.

5 ANALYSIS RESULTS

The CAR-MHF process was performed on data spanning the 2 week period of January 7-21 2010. No specific *a priori* orbit or AMR information was provided to CAR-MHF beyond the constraints that the semi-major axis have values between 33000-45000 km, that the eccentricity be less than 0.2 and the AMR fall in the range of 0-5 m^2/kg.

The results are summarized in Table 3 below where the object number in the far left column indicates which HAMR debris object the results represent (as compared to the ODTK analyses). The number of starting hypotheses generated by CAR, and the "final" number of hypotheses are indicated in columns 2 and 3. Columns 4 and 5 show the total number of observation pairs (right ascension and declination) that were associated to each object, and of those, the number of false associations. Columns 6 and 7 are the averages

(over 2009-2010) and CAR-MHF solutions for semi-major axis. Columns 8-10 are the averages (over 2009-2010), variations of the averages and the CAR-MHF solutions for inclination. Similarly, columns 11-13 are the averages (over 2009-2010), variations of the averages and CAR-MHF solutions for eccentricity. And finally, columns 14-16 are the corresponding averages (over 2009-2010), variations and CAR-MHF solutions for CrA/m. A synopsis of the results presented in Table 3 are subsequently provided.

It is first noted that the majority of objects converged to the expected solutions (un-colored rows), and most of those converged to a single hypothesis, with a few having 2-3 remaining hypotheses. Subsequent data for these latter objects would likely allow those also to converge to a single hypothesis. It is noted that, though Object #60 had 6 false associations, the Probabilistic Data Association (PDA) weighting evidently prevented the solution from diverging. Most all CAR-MHF solutions at the last observation fall within the average, plus or minus the variation, with one exception. Object #80, highlighted in the darker blue row, did not converge to the correct CrA/m value in spite of no false association. Further analysis revealed that this object had data only spanning 1-2 days and, hence, was of insufficient duration to "observe" the CrA/m. Subsequent data spanning a longer duration would likely help the solution to converge to the correct value, provided the subsequent data were correctly associated.

There were several cases where a single object had a second CAR generated, and observations processed. Object #83, highlighted in yellow rows, is one of these. In this case, there was a gap in the data which resulted in the object's estimate being terminated (a user-defined "kill" rule). A subsequent set of observations resulted in a new CAR being generated, and the data after that point being correctly associated. One can see that the solutions match quite nicely and, with the aid of backward smoothing, would certainly be combined into a single estimate upon subsequent filtering.

Object #96 is another instance where two CARs were generated for a single object. However, in this case, the first CAR (highlighted in the red row) had a relatively small amount of data associated with it, and of these, a significant percentage were false associations. The second instance (highlighted in the yellow row) has more data associated with it, and no false associations, and with sufficient follow-up data would likely converge to the correct solution as indicated by the results at the end of the processing.

The last object having duplicate CARs generated and subsequent estimates is Object #97 (both highlighted in red rows). In this case, the number of observations associated was small and, having no follow-up data in a reasonable amount of time, resulted in these two "false starts."

Finally, Object #65 (highlighted as a red row) had very little data for the filter to follow-up on, with 8 associated observations and 2 of those false. This estimate would not likely result in further correct associations and, subsequently, the estimate would be "killed" with no legitimate follow-up data after a specified time.

Table 3. CAR-MHF results are provided for the 26 near GEO HAMR objects for processing over Jan. 7-21, 2010.

1	2	3	4	5	6	7	8	9	10	11	12	13	14	15	16
HAMR Obj. #	Start # Hypoth.	End # Hypoth.	# Assoc. Obs.	# False Assoc.	Avg. Sma (km)	CAR-MHF Sma (km)	Avg. Inc. (deg)	Var. Inc. (deg)	CAR-MHF Inc. (deg)	Avg. Ecc	Var. Ecc	CAR-MHF Ecc.	Avg. CrA/m (m^2/kg)	Var. CrA/m (m^2/kg)	CAR-MHF CrA/m (m^2/kg)
60	528	1	255	6	39990	39990	11.9	0.9	11.8	0.135	0.110	0.186	3.340	0.010	3.260
61	732	1	62	0	42618	42620	14.7	0.2	14.7	0.011	0.003	0.009	0.097	0.070	0.032
63	681	1	72	0	38230	38215	6.4	1.7	6.3	0.085	0.150	0.084	4.881	0.060	4.847
64	774	1	71	0	40402	40392	8.8	0.7	8.9	0.071	0.139	0.127	4.308	0.220	4.428
65	712	14	8	2	42239	33226	14.9	0.1	14.5	0.023	0.034	0.164	1.222	0.750	2.542
67	694	1	234	0	41584	41588	13.2	0.2	13.3	0.045	0.030	0.039	0.985	0.180	0.980
68	894	1	146	0	40790	40787	13.2	0.1	13.1	0.035	0.030	0.051	1.044	0.700	0.569
71	697	1	150	0	41469	41473	13.2	0.3	13.1	0.016	0.029	0.018	0.802	0.330	0.782
73	827	1	44	0	40374	40374	12.0	0.2	12.0	0.055	0.010	0.053	0.489	0.270	0.371
77	617	1	86	0	41424	41420	13.0	0.6	13.0	0.045	0.071	0.058	2.073	0.350	2.036
79	721	2	50	0	45135	45130	19.7	0.1	19.7	0.105	0.050	0.114	2.952	0.030	2.915
80	685	1	28	0	41843	41840	7.8	1.0	7.7	0.038	0.064	0.071	2.884	0.010	0.001
82	635	3	51	0	39729	39734	8.5	0.8	8.5	0.055	0.070	0.070	2.137	0.070	2.037
83	590	2	63	0	44704	44695	16.8	0.1	16.8	0.090	0.060	0.102	2.075	0.110	1.901
83	290	1	89	0	44704	44695	16.8	0.1	16.8	0.090	0.060	0.102	2.075	0.110	1.888
84	750	2	25	0	41922	41915	14.2	0.1	14.2	0.013	0.015	0.005	0.881	0.010	0.822
85	792	1	169	0	42446	42446	14.7	0.1	14.7	0.040	0.020	0.037	0.491	0.180	0.258
86	440	3	84	0	42448	42450	16.0	0.1	16.0	0.060	0.080	0.100	2.165	0.090	2.302
87	(no data)	(no data)	(no data)	(no data)	33194	(no data)	10.0	0.1	(no data)	0.275	0.010	(no data)	3.636	0.050	(no data)
90	833	2	102	0	40121	40124	12.1	0.2	12.1	0.031	0.059	0.010	1.687	0.090	1.622
93	589	1	84	0	40181	40178	10.9	0.8	10.9	0.095	0.050	0.121	1.548	0.450	1.170
94	772	1	103	0	41311	41300	9.7	1.2	10.3	0.056	0.108	0.016	3.305	0.030	3.242
95	633	3	36	0	41171	41363	13.9	0.1	13.9	0.035	0.010	0.059	2.800	1.200	1.578
96	690	1	19	11	41308	41284	12.9	0.2	12.7	0.040	0.020	0.107	0.837	0.700	4.792
96	714	1	29	0	41308	41300	12.9	0.2	13.0	0.040	0.020	0.030	0.837	0.700	0.543
97	742	4	12	4	41461	33573	13.4	0.3	13.3	0.014	0.013	0.051	0.786	0.260	2.658
97	742	6	14	4	41461	31052	13.4	0.3	13.6	0.014	0.013	0.233	0.786	0.260	2.544
98	851	2	12	4	46228	29642	18.7	0.1	19.2	0.125	0.050	0.231	3.133	2.300	2.469
99	659	1	109	0	44626	44625	19.9	0.5	19.9	0.095	0.050	0.097	1.356	0.020	1.324

The summary above provides just an overview of the results, and indicates the overall successful performance of CAR-MHF in finding and determining orbit and AMR values autonomously with no *a priori* orbit or AMR values. A more detailed look at one of the objects (Object #60) is now provided in order to yield some insight into the results.

The tracking data history for Object #60 over a 1-week span is shown in Figure 9. The CAR initializes on the first data available on January 7, and it would have to be "rejected" in the data association of any CARs initiated previously.

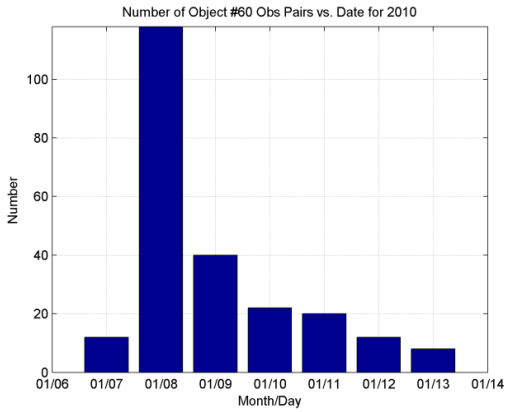

Figure 9. Example measurement distribution example for Object #60 over the week Jan. 7-14, 2010.

The CAR and associated hypotheses for Object #60 are shown in Figure 10, where the admissible region (range-rate vs. range) is shown in green in the plot on the left-hand side, and the plots on the right show the "discretized" hypotheses corresponding to the orbit eccentricity vs. semi-major axis (top), inclination versus semi-major axis (middle) and right ascension of ascending node versus semi-major axis). These are derived from the initial angle tracklet and derived angle rates [8], the orbit constraints and the non-linear mapping from angle, range and range-rate to Cartesian J2000 position and velocity (and, hence, Classical elements). The AMR constraints also add additional hypotheses that the MHF processes.

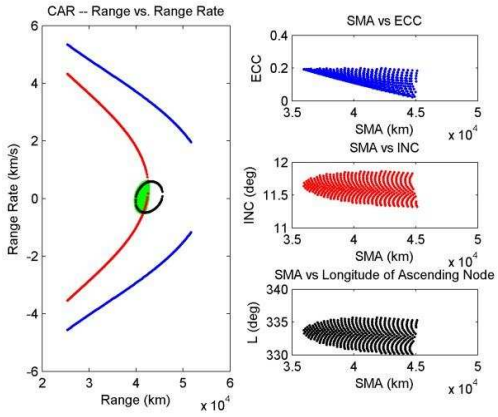

Figure 10. Example Constrained Admissible Region (CAR) and associated hypotheses for Object #60.

In this case, the several hundred Object #60 initial hypotheses were reduced to a single hypothesis after 2-3 days of data processing. The converged orbit and AMR values are as follows:

a = 39998.565 km
e = 0.1841
i = 11.820 deg
L = 331.129 deg
w = 349.442 deg
ta = 140.182 deg
CrA/m = 2.981 m^2/kg

One can compare to the "truth" values provided in Table 1 and see that these osculating state elements fall within the averages and associated variations. Plots of the estimation history of the semi-major axis, eccentricity, inclination and right ascension of ascending node are provided in Figure 11 for the first week of processing. The AMR estimation history, and its associated uncertainty, are provided in Figure 12 where it can be seen that it appears to converge to a fairly stable value after about 3 days of processing.

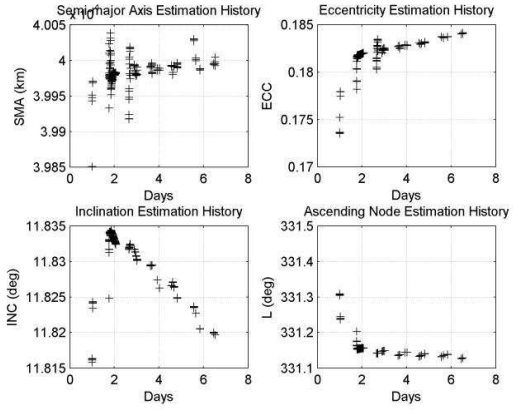

Figure 11. Example element estimation history (semi-

major axis, eccentricity, inclination and RAAN) for Object #60 over the 7-day estimation period.

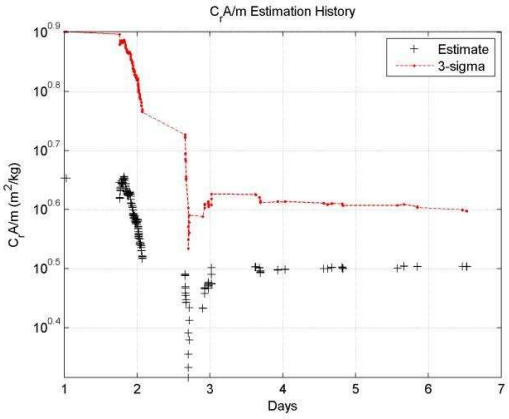

Figure 12. Example CrA/m estimation history for Object #60 over the 7-day estimation period.

6 SUMMARY AND CONCLUSIONS

The CAR-MHF approach to initial orbit determination and object characterization was applied to a set of HAMR debris objects and compared to previously determined results for those objects. No *a priori* orbit and CrA/m values were used beyond constraints enforced for the hypothesis generation in the CAR. The results show the overall successful performance of CAR-MHF in finding and determining orbit and AMR values autonomously with no *a priori* orbit or AMR values. There were some cases where data were incorrectly associated, but the PDA approach de-weighted many of these and good solutions were achieved. There was one case where insufficient data were available to converge to the correct orbit and CrA/m solution, and another where there was insufficient duration of data for the CrA/m estimate to converge to the correct value. Lastly, there were a few cases where duplicate CARs were generated, along with subsequent solutions. These were due to gaps in the data causing estimates to be terminated, and subsequently, new estimates to be generated. Some of this could also be affected by significant variations in the CrA/m causing mis-associations to occur, and a new track thus generated. The tracks would ultimately be correlated with the aid of backward smoothing.

Some of the shortcomings noted in the PDA approach will be mitigated by several future modifications. Implementation of Joint Probabilistic Data Association (JPDA) will allow for a more efficient, statistically consistent and robust data association. Compressing tracklets to a single measurement will also aid in mitigating the cases where an outlier causes a false association and, hence, initiation of a new CAR when subsequent data might be correctly associated for an object. Finally, in the cases where there are sparse data, and/or long periods between observations, correctly characterizing the errors should improve the data association performance [11]. Future work will be expanded to include other orbit regimes, including geosynchronous transfer orbits (GTO) which can have segments passing through GEO.

7 ACKNOWLEDGE ENTS

We would like to acknowledge the U.S. Air Force Space Command for supporting this work, and specifically, Robin Thurston for providing the data. We also wish to thank the Air Force Research Laboratory for funding most of the work presented here.

8 REFERENCES

1. Schildknecht, et al. (2005). Properties of the High Area-to-mass Ratio Space Debris Population in GEO," AMOS Technical Conference. Wailea, Hawaii, Sept, 2005.

2. Kelecy, T., T. Payne, R. Thurston and G. Stansbery (2007). Solar Radiation Pressure Estimation and Analysis of a GEO Class of High Area-to-mass Ratio Debris Objects. AAS 07-391, AAS Astrodynamics Specialist Conference, Mackinac Island, MI, August 2007.

3. Kelecy T., E. Barker, P. Seitzer, T. Payne and R. Thurston (2008). Prediction and Tracking Analysis of a Class of High Area-to-mass Ratio Debris Objects in Geosynchronous Orbit. AMOS Technical Conference., Wailea, Hawaii, Sept, 2008.

4. Kelecy, T. and M. Jah (2009). Analysis of Orbit Prediction Sensitivity to Thermal Emissions Acceleration Modeling for High Area-to-mass Ratio (HAMR) Objects. AMOS Technical Conference, Wailea, Hawaii, Sept, 2009.

5. Hujsak, R., J.Woodburn, J. Seago (2007). The Orbit Determination Tool Kit (ODTK) – Version 5. AAS 07-125, AAS Astrodynamics Specialist Conference, Mackinac Island, MI, August 2007.

6. DeMars and K., M. Jah (2009). Passive Multi-Target Tracking with Application to Orbit Determination for Geosynchronous Objects. AAS Paper 09-108, 19th AAS/AIAA Space Flight Mechanics Meeting, Savannah, Georgia, February 8-12, 2009.

7. Milani, A., G. Gronchi, M.D.M. Vitturi and Z. Knezevic (2004). Orbit Determination with Very Short Arcs. I Admissible Regions. Celestial Mechanics and Dynamical Astronomy, Vol. 90, July 2004, pp59-87.

8. Kelecy, T., M. Jah and K. DeMars (2012). Application of a Multiple Hypothesis Filter to near GEO high area-to-mass ratio space objects state

estimation. Acta Astronautica, 81, pp 435-444.

9. DeMars, K., M. Jah and P. Schumacher (2012). Initial Orit Determination using Short-Arc and Angle Rate Data. IEEE Journal of Transactions on Aerospace and Electronic Systems, Volume 48, Number 3, July 2012.

10. Julier, S. and J. K. Uhlmann (1997). A New Extension of the Kalman Filter to Nonlinear Systems. Proceedings of the SPIE – The International Society for Optical Engineering, Vol 3068, April 1997, pp 182-193.

11. DeMars, K., M. Jah, D. Giza and T. Kelecy (2009). Orbit Determination Performance Improvements for High Area-to-mass Ratio Space Object Tracking using and Adaptive Gaussian Mixtures Estimation Algorithm, 21st International Symposium on Space Flight Dynamics (ISSFD), Toulouse, France, Sep-Oct 2009.